Journal of Sound and Vibration 517 (2022) 116538

Contents lists available at ScienceDirect

Journal of Sound and Vibration

journal homepage: www.elsevier.com/locate/jsvi

Bi-stability induced by motion limiting constraints on boring bar tuned mass dampers

Zsolt Iklodi [a,*], David A.W. Barton [b], Zoltan Dombovari [a]

[a] MTA-BME Lendület Machine Tool Vibration Research Group, Department of Applied Mechanics, Budapest University of Technology and Economics, Budapest H-1521, Hungary

[b] Department of Engineering Mathematics, University of Bristol, Bristol, United Kingdom

ARTICLE INFO

Keywords:
Chatter
Tuned mass damper
Piecewise-smooth
Impact
Fly-over
Continuation

ABSTRACT

This paper investigates the effect of displacement constraints on the attenuation performance of tuned mass dampers (TMDs) used in boring and turning applications. A simplified piecewise-smooth mechanical model is investigated through time domain simulations and hybrid periodic orbit continuation, first under harmonic excitation, then under regenerative cutting load. A quasi-frequency response function is derived for impacting TMDs through composition of different families of period-1 orbits, then an acceptability map for turning is formulated based on the appearance of cutting-edge contact-loss and fly-over events. The bi-stable domain boundaries are determined through two parameter continuation of contact-loss grazing events. It is shown that in both cases arising rigid body collisions can significantly hinder TMD damping performance and lead to resonance problems or machine tool chatter.

1. Introduction

Tuned mass dampers have been successfully implemented in industrial machining solutions [1,2], such as the boring bars discussed in [3]. These TMDs with the optimal tuning induce a significant increase in the stable regions of the regeneration–delay stability charts, while also raising the critical depth of cut, similarly to Fig. 1.(c). Consequently, material removal rate and the tool length to diameter ratio can both be increased compared to regular boring bars, while maintaining safe, chatter free operation.

The use of tuned-mass dampers (TMDs) is a simple and powerful approach to solve industrial resonance problems. In principle installing a mass and spring system with optimal tuning can completely cancel out resonant vibrations by utilizing the antiresonance phenomenon. Unfortunately, in practice this simple solution is only applicable when the natural frequency of the system and the operational bandwidth of excitation is constant and known. In machining applications both of these parameters often vary due to changing spindle speeds or tooling and fixture configurations.

If during operation, the operational frequency deviates from the point of antiresonance the aforementioned device suffers a sharp deterioration in its attenuation performance [4], which becomes even more significant as the newly introduced resonant frequency is approached. To overcome this issue, Den Hartog [5] showed that by introducing a certain amount of damping the operational frequency range can be greatly expanded with a relatively small sacrifice of absorber performance, thus introducing the concept of the modern TMD. Den Hartog also derived closed form expressions for the optimal tuning of such devices to achieve the lowest vibration amplitude across the whole excitation frequency range.

In machining applications the stability of cutting and the appearance of unwanted harmful vibrations (chatter) is connected in a simplified manner to the real part of the frequency response function (FRF) of the machine tool. Consequently, as shown by Sims [6]

* Corresponding author.
E-mail address: zsolt.iklodi@mm.bme.hu (Z. Iklodi).

https://doi.org/10.1016/j.jsv.2021.116538
Received 22 June 2021; Received in revised form 31 August 2021; Accepted 5 October 2021
Available online 13 October 2021

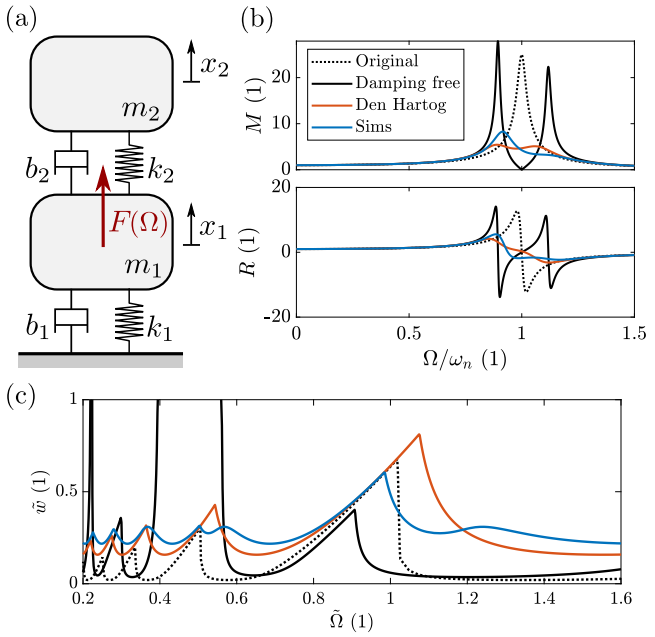

Fig. 1. Comparison of TMD tunings. Panel (a) shows the mechanical model of the TMD designed to reduce resonant vibrations of m_1. Panel (b) presents the absolute value (M) and real part (R) of the resulting system dimensionless FRFs $\left(\frac{X_1(\Omega)}{m_1\omega^2 F(\Omega)}\right)$, while panel (c) shows the spindle speed - depth of cut stability charts of turning based on these FRFs.

optimizing the TMD tuning for minimizing either peak of the FRF's real part, the robustness of the cutting process can be increased even further. Since this tuning method provides the highest critical depth of cut, below which the operation is stable on the entire spindle speed domain, it is frequently used in TMDs designed for machining applications.

A comparison of the discussed tuning methods (damping free, Den Hartog, Sims) is presented on Fig. 1. As seen here on panel (b) and (c), tuning for antiresonance results the highest peaks in the real part of the FRF and consequently leads to the lowest critical depth of cut, making it inconvenient for machine tools.

In boring applications, for optimal performance, tuned mass dampers have to be placed close to the cutting edge [7,8]. Due to the lack of space, this means installing the TMD inside a tube segment of the boring bar. This is a simple and effective technique, however it also weakens the structure of the bar and restricts the free displacement of the TMD.

Given large enough tool vibrations these constructional constraints will lead to inevitable collisions between the TMD and the inner surface of the boring bar, after which the system becomes non-linear and piecewise-smooth. Intuitively it is unclear how this will affect the absorbing performance of the TMD. On one hand the restriction of the TMD will lead to less energy displaced to the additional TMD mode and dissipated through viscose damping, but on the other hand the inelastic impacts might be able to compensate for it.

As demonstrated in several studies, the energy dissipated during rigid body collisions is a practical approach of vibration attenuation and chatter suppression for boring and turning operations. The effectiveness of impact dampers is shown by bending, impact, and cutting tests in [9], by a neural network based tool-wear predictor in [10], and by analytic investigation using the method of multiple scales in [11]. With high vibration amplitudes the constrained TMD will behave and dissipate energy similarly to these impact dampers.

This paper aims to uncover how the arising impacts affect the stability maps of turning and boring. As is common in the literature [3,8,11] to emphasize the underlying behaviour, the machine tool assembly is reduced to a 2 degree of freedom (DoF) piecewise-linear vibro-impact oscillator, focusing only on the first, most dominant mode.

The dynamic behaviour of low-DoF vibro-impact oscillators has been thoroughly researched. In [12,13], hybrid return maps and Floquet theory are employed to investigate a flexible beam subjected to rigid amplitude constraints and a constrained inverted pendulum placed on a linear oscillator respectively. In [14], the shooting method is employed for bifurcation analysis of the free vibrations of a conservative 2-DoF piecewise-linear vibro-impact oscillator. Sticking solutions and Zeno behaviour (impact chatter) are investigated in [15,16] by detailed numerical studies.

Such mechanical systems are often described by their piecewise-smooth periodic orbits, built up from continuous segments separated by discrete impact events (hybrid-periodic orbits). These can be analysed through piecewise-smooth Poincaré return maps [12,13], shooting methods [14] or collocation [17]. They exhibit rather intricate dynamic phenomena, such as grazing and sliding bifurcations, Zeno behaviour (often called chatter), and sudden transitions to chaos. Due to high parameter sensitivity and discontinuous changes in system dynamics, both numerical and analytic investigation requires a great deal of effort and care.

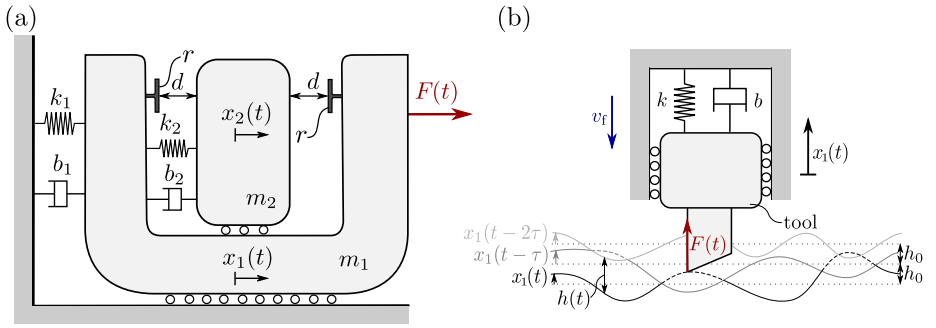

Fig. 2. Panel (a) piecewise-linear vibro-impact oscillator model. Panel (b) calculation of actual feed rate accounting for contact loss events and fly-over modes. $h(t) = 0$ in fly-over segments denoted by dashed lines.

Applying the aforementioned methods to the mechanical model of boring with a constrained TMD is far from straightforward. The cutting forces introduce a regenerative effect, which converts the governing equation of motion into a piecewise-smooth delay differential equation, and on high vibration amplitudes, the possible contact loss of the cutting edge also has to be accounted for. This leads to a new non-smooth event and requires the storing of workpiece profiles from past revolutions [18,19].

There are open source continuation packages available for hybrid-dynamic systems (which have both continuous and discrete dynamics) such as PyDSTool [20], TC-HAT [17] and the COCO hpo package [21]. However, for the level of customizability needed in this application, a problem specific hybrid periodic orbit correction and continuation scheme was written. Since the phase space of delay differential equations is infinite dimensional, the shooting and Poincaré return map methods require some form of discretization in time. Consequently, spectral collocation was used for the analysis and continuation of hybrid periodic orbits, as it provides good convergence properties [22,23] and the orbit has to be discretized either way.

Aided and guided by time domain simulation results, the developed spectral collocation scheme was first used on the piecewise-linear vibro-impact oscillator model, in the presence of harmonic excitation. By following period-1 orbits with different number of impacts, a quasi-frequency response function was constructed for the constrained TMD. Then the numerical methods were generalized to account for delayed terms, contact-loss events, and fly-over modes. An approximate non-smooth stability map of turning was formulated through time domain simulations, and was validated by two parameter continuation of hybrid periodic orbits with grazing bifurcations on the event surface of cutting edge contact-loss.

The remainder of this paper is structured as follows. In Section 2 the mechanical model of boring with a constrained tuned mass damper is derived, accounting for rigid body collisions, cutting edge contact-loss and fly-over modes. Section 3 discusses the time domain simulation routines, the boundary value problem formulation of hybrid periodic orbits, and the operation of the continuation algorithm. Section 4 displays the results achieved by these numerical methods, and finally Section 5 presents conclusions.

2. Model description

When formulating the mechanical model of boring with a constrained TMD, only the first, dominant mode of the machine tool assembly was taken into account, thus reducing the problem to the 2 DoF piecewise-linear vibro-impact oscillator shown on Fig. 2(a). Here m_1, b_1 and k_1 represent the modal mass, damping and stiffness of the machine tool, m_2, b_2 and k_2 are the TMD mass, damping and stiffness, while d is the TMD clearance and r is the coefficient of restitution. The $F(t)$ excitation will later represent either a harmonic load or the regenerative cutting force.

Considering instantaneous, inelastic impacts according to the Newton's impact law, the governing equation of motion is

$$\begin{aligned}
&\text{if } |x_1 - x_2| < d \\
&\qquad \begin{bmatrix} m_1 & 0 \\ 0 & m_2 \end{bmatrix} \begin{bmatrix} \ddot{x}_1 \\ \ddot{x}_2 \end{bmatrix} + \begin{bmatrix} b_1 + b_2 & -b_2 \\ -b_2 & b_2 \end{bmatrix} \begin{bmatrix} \dot{x}_1 \\ \dot{x}_2 \end{bmatrix} + \begin{bmatrix} k_1 + k_2 & -k_2 \\ -k_2 & k_2 \end{bmatrix} \begin{bmatrix} x_1 \\ x_2 \end{bmatrix} = \begin{bmatrix} F(t) \\ 0 \end{bmatrix}, \\
&\text{if } |x_1 - x_2| = d \\
&\qquad \begin{bmatrix} \dot{x}_1^+ \\ \dot{x}_2^+ \end{bmatrix} = \begin{bmatrix} \frac{m_1(r+1)}{m_1+m_2} - r & \frac{m_2(r+1)}{m_1+m_2} \\ \frac{m_1(r+1)}{m_1+m_2} & \frac{m_2(r+1)}{m_1+m_2} - r \end{bmatrix} \begin{bmatrix} \dot{x}_1^- \\ \dot{x}_2^- \end{bmatrix}.
\end{aligned} \tag{1}$$

For the representation of the regenerative cutting force, a simple linear orthogonal cutting model was used

$$F(t) = K_{cr} w h(t), \tag{2}$$

where K_{cr} is the radial cutting edge coefficient, w is the depth of cut and $h(t)$ is the actual feed rate. Considering large vibrations and fly-over segments, $h(t)$ can be calculated as illustrated on Fig. 2(b).

$$\bar{h}(t) = \min_k (k h_0 - x_1(t) + x_1(t - k\tau)),$$
$$h(t) = \begin{cases} 0, & \text{if } \bar{h}(t) < 0, \\ \bar{h}(t), & \text{if } \bar{h}(t) \geq 0, \end{cases} \tag{3}$$

where $k = 1, 2, \ldots, n$, v_f and $h_0 = \frac{2\pi}{\Omega} v_f$ is the prescribed feed and feed rate, while $\tau = \frac{2\pi}{\Omega}$ is the time needed for one full workpiece revolution.

To reduce the number of system parameters, Eq. (1) can be nondimensionalized using the inverse of the natural frequency of the dominant mode of the machine tool as a time unit $\tilde{t} := \omega_1 t = \sqrt{\frac{k_1}{m_1}} t$, and either the equilibrium clearance or the prescribed feed rate as a displacement unit. Consequently the two excitation cases considered will take the following forms

$$\tilde{d} := 1, \quad f(\tilde{t}) := f \cos(\Omega \tilde{t} + \phi), \quad f := \frac{F}{\omega_1^2 m_1 d}, \tag{4}$$

for harmonic ($\tilde{x} := \frac{1}{d}$), and

$$\tilde{d} := \frac{d}{h_0}, \quad f(\tilde{t}) := \tilde{w} \tilde{h}(\tilde{t}), \quad \tilde{w} := \frac{K_{cr} w}{\omega_1^2 m_1}, \quad \tilde{h}(\tilde{t}) := \frac{h(\tilde{t})}{h_0}. \tag{5}$$

for regenerative cutting force ($\tilde{x} := \frac{1}{h_0} x$). Dropping the tildes results in the nondimensionalized equation of motion

$$\begin{aligned} &\text{if } |x_2 - x_1| < d \\ &\qquad \begin{bmatrix} 1 & 0 \\ 0 & \mu \end{bmatrix} \begin{bmatrix} \ddot{x}_1 \\ \ddot{x}_2 \end{bmatrix} + \begin{bmatrix} 2\zeta + 2\chi\mu & -2\chi\mu \\ -2\chi\mu & 2\chi\mu \end{bmatrix} \begin{bmatrix} \dot{x}_1 \\ \dot{x}_2 \end{bmatrix} + \begin{bmatrix} 1 + \varphi^2\mu & -\varphi^2\mu \\ -\varphi^2\mu & \varphi^2\mu \end{bmatrix} \begin{bmatrix} x_1 \\ x_2 \end{bmatrix} = \begin{bmatrix} f(t) \\ 0 \end{bmatrix}, \\ &\text{if } |x_2 - x_1| = d \\ &\qquad \begin{bmatrix} \dot{x}_1^+ \\ \dot{x}_2^+ \end{bmatrix} = \begin{bmatrix} \frac{r+1}{1+\mu} - r & \frac{\mu(r+1)}{1+\mu} \\ \frac{r+1}{1+\mu} & \frac{\mu(r+1)}{1+\mu} - r \end{bmatrix} \begin{bmatrix} \dot{x}_1^- \\ \dot{x}_2^- \end{bmatrix}, \end{aligned} \tag{6}$$

where $\zeta := \frac{b_1}{2\omega_1 m_1}$ is the oscillator damping ratio.

The tuned mass damper frequency tuning $\varphi := \frac{\omega_2}{\omega_1} = \frac{\sqrt{k_2/m_2}}{\sqrt{k_1/m_1}}$ and stand-alone damping ratio $\chi := \frac{b_2}{2\omega_1 m_2}$ is assumed to be tuned according to the closed form formulas of Sims [6]

$$\varphi = \sqrt{\frac{\mu + 2 + \sqrt{2\mu + \mu^2}}{2(1+\mu)^2}}, \quad \chi = \sqrt{\frac{3\mu}{8(1+\mu)}}, \tag{7}$$

with the mass ratio $\mu = \frac{m_2}{m_1}$ as a given parameter.

Sims tuning was selected as it provides the highest critical depth of cut for the simple turning operation, as seen on Fig. 1.(c), and its frequently used in commercially available boring bars [3]. A major part of this paper is devoted to show how the performance of these devices deteriorates from the results of linear stability analysis when displacement constraints are accounted for.

3. Numerical methods

For displacement constrained TMDs, the governing equation of motion (6) is a hybrid, piecewise-linear ordinary (ODE) or delay differential equation (DDE), depending on the form of excitation: (4) or (5). Investigating such equations is often too complicated to do so analytically, therefore numerical methods are employed for the analysis of system dynamics. This section presents the numerical methods used for time domain simulation and hybrid periodic orbit continuation of Eq. (6).

3.1. Time domain simulation

To get a general feel of system dynamics, first a time domain simulation scheme was formulated, exploiting the ODE/DDE solver and event handling functionalities of the *DifferentialEquations.jl* [24] *Julia* package.

First, Eq. (6) was converted to first order form using $\mathbf{u} = [x_1,\ x_2,\ \dot{x}_1,\ \dot{x}_2]^\intercal$. On smooth segments, this results in

$$\dot{\mathbf{u}} = \mathbf{A}\mathbf{u} + \mathbf{b}, \tag{8}$$

where

$$\mathbf{A} = \begin{bmatrix} 0 & 0 & 1 & 0 \\ 0 & 0 & 0 & 1 \\ -1 - \varphi^2\mu & \varphi^2\mu & -2\zeta - 2\chi\mu & +2\chi\mu \\ \varphi^2 & -\varphi^2 & 2\chi & -2\chi \end{bmatrix}$$

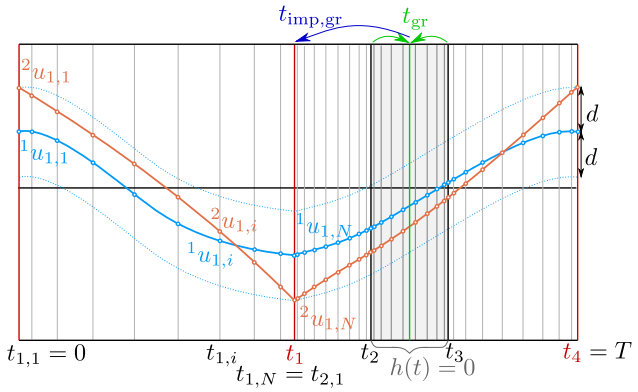

Fig. 3. Boundary value problem formulation of hybrid periodic orbits of turning with a constrained tuned mass damper. Using a scaled Chebyshev mesh of size N, on n segments with m coordinate dimensions. Therefore, $i = 1 \dots N$, $j = 1 \dots n$, $k = 1 \dots m$, and the orbit is described by ${}^k u_{j,i}$ state variables and t_j event times. Blue and orange lines show the first two dimensions of the state in a possible orbit ($n = 4$, $N = 10$, $m = 4$). The grey area denotes the time spent in fly-over, which in some cases can be reduced to the green grazing point. If this coincides with an impact event a blue double event point can be formulated. (For interpretation of the references to colour in this figure legend, the reader is referred to the web version of this article.)

and $\mathbf{b} = [0,\ 0,\ f(t),\ 0]^{\mathrm{T}}$, and at non-smooth event times ($|u_2 - u_1| = d$) the impact map becomes

$$\mathbf{u}^+ = \mathbf{R}\mathbf{u}^-, \tag{9}$$

with

$$\mathbf{R} = \begin{bmatrix} 1 & 0 & 0 & 0 \\ 0 & 1 & 0 & 0 \\ 0 & 0 & \frac{r+1}{1+\mu} - r & \frac{\mu(r+1)}{1+\mu} \\ 0 & 0 & \frac{r+1}{1+\mu} & \frac{\mu(r+1)}{1+\mu} - r \end{bmatrix}.$$

To simulate the solution of (6), Eq. (8) was integrated using the *Tsit5* (Tsitouras 5/4 Runge–Kutta) method, while detecting and applying (9) when a zero crossing is found in the impact condition using a root finding algorithm.

Most of the time this provided adequate results, however due the appearance of Zeno behaviour (impact chatter), with the available limited numerical precision, impact events sometimes went undetected, leading to solutions with no physical meaning. As demonstrated by Nordmark and Piiroinen [25] these infinite impact sequences can be detected, and their completion, which requires a finite amount of time, can be predicted. If chatter events are complete, the solution will transition to a sliding one, where the two degrees of freedom evolve in unison until a separation condition is met.

Consequently an additional condition was implemented in the event handling algorithm, to check for possible chatter sequences. If $\Delta t_i < \epsilon$, where Δt_i is the time elapsed between two subsequent impacts, the integration is stopped and continued as a sliding solution, determined by integrating

$$\dot{\mathbf{u}}^* = \frac{1}{1+\mu}\left(\begin{bmatrix} 0 & 1 \\ -1 & -2\zeta \end{bmatrix}\mathbf{u}^* + \begin{bmatrix} 0 \\ f(t) \end{bmatrix}\right) \tag{10}$$

until the separation condition $\dot{u}_2^* = \pm\varphi^2 d$ is reached. This corresponds to the time instant when the spring force of k_2 overcomes the inertial force. Here $\mathbf{u}^* = [u_1,\ u_3]^{\mathrm{T}}$, which at the end is transformed back as $\mathbf{u} = [u_1^*,\ u_1^* \pm d,\ u_2^*,\ u_2^*]^{\mathrm{T}}$, depending on which event surface, the complete impact chatter phenomenon took place on. Finally the integration of (8) is resumed in the aforementioned fashion.

3.2. Boundary value problem of hybrid periodic orbits

Time domain simulation is a powerful tool, however due to the non-linear, initial condition and parameter dependent behaviour of Eq. (6), cannot provide a reliable general picture of system dynamics. For further numerical analysis a hybrid periodic orbit continuation scheme was formulated, based on the spectral collocation methods described by Trefethen in [22].

Periodic orbits of initial value problems can also be obtained as solutions of appropriate boundary value problems (BVPs), with infinite-dimensional boundary conditions in the case of DDEs [26]. For periodic orbits of piecewise-smooth systems, the same can be achieved, either through smoothing the non-smooth effects [19], or applying inner boundaries for all such events [18].

First of all, formulating the appropriate BVP requires the adequate discretization of the hybrid periodic orbits. As the solution on the smooth segments of orbits is generally not periodic, the use of Chebyshev polynomials is a straightforward choice. It provides a homogeneous interpolation within the intervals, and allows spectral differentiation, which converges fast and is easily rescalable with interval lengths.

Table 1
List of event and segment boundary types considered, illustrated with the same colours on Fig. 3. The condition column defines the event surface, while the boundary column describes the smooth or non-smooth event map.

	Name	Condition	Boundary
●	impact	$\lvert {}^{2}u_{j,N} - {}^{1}u_{j,N}\rvert = d$	$\mathbf{u}_{j+1,1} = \mathbf{R}\mathbf{u}_{j,N}$
●	contact-loss	$1 - {}^{1}u_{j,N} + {}^{1}u(t_{j,\tau})$	$\mathbf{u}_{j+1,1} = \mathbf{u}_{j,N}$
●	contact-loss grazing	$1 - {}^{1}u_{j,N} + {}^{1}u(t_{j,\tau})$ $-{}^{j}u_{3}^{N} + {}^{3}u(t_{j,\tau})$	$\mathbf{u}_{j+1,1} = \mathbf{u}_{j,N}$
●	impact and contact-loss grazing	$\lvert {}^{j}u_{2}^{N} - {}^{1}u_{j,N}\rvert = d$ $1 - {}^{1}u_{j,N} + {}^{1}u(t_{j,\tau})$ $-{}^{3}u_{j,N} + {}^{3}u(t_{j,\tau})$	$\mathbf{u}_{j+1,1} = \mathbf{R}\mathbf{u}_{j,N}$

The first step of discretization is to assign segment boundaries to each non-smooth event, as illustrated in Fig. 3. By default this can either be an impact, or a contact-loss event. Later on, for two parameter continuation, more complicated contact-loss grazing, and impact contact-loss grazing boundaries will be defined as well. These points all come with one or more conditions to ensure their existence, and a continuity law, which will provide the necessary boundary conditions for proper formulation of the BVP. These event types and their respective constraints are listed on Fig. 1. Since these events and consequently the segment boundaries are allowed to move, their times are included as free variables when formulating the governing BVP. The event conditions provide the extra constraints necessary to keep it fully defined.

Now the only thing left to do is to apply the continuously smooth equation of motion (8) for the inner points of each segment. This was achieved using the first $N-1$ rows and all N columns of the Chebyshev spectral differentiation matrix $\mathbf{D}$ defined in chapter 6 of [22]. Doing so results in the following set of $(N-1)\times n\times m$ equations

$$\frac{2}{t_j - t_{j-1}}\mathbf{D}\,{}^{k}\mathbf{u}_{j,i} = \mathbf{A}\,{}^{k}\mathbf{u}_{j,i} + \mathbf{b}(t_{j,i}), \tag{11}$$

where $i = 1,\dots,N-1$ is the mesh index within smooth segments, $j = 1,\dots,n$ is the index of segments within the orbit, and $k = 1,\dots,m$ indexes the coordinate dimensions. Assuming an m coordinate dimensions ($m = 4$ in this case), on n smooth segments, with N mesh points in each. In (11), all N mesh points are necessary for the spectral derivation, however in the BVP only $N-1$ equations are considered as the Nth terms are be defined by the boundary conditions provided in Table 1. Due to the periodicity of the orbits, $j-1$ maps to n if $j = 0$ and $j+1$ maps to 1 for $j = n$.

Unfortunately the calculation of $\mathbf{b}(t_{j,i})$ is not trivial, especially in the regenerative case. If $\mathbf{b}(t_{j,i})$ is defined using (4), assuming harmonic excitation, the calculation requires an extra phase variable ϕ, and consequently an additional phase condition $t_n = l\frac{2\pi}{\Omega}$, $l \in \mathbb{N}$.

When the regenerative force from Eq. (5) is considered, the calculation of $f(t)$ is not so straightforward. Evaluating the actual feed rate is rather complicated, especially when contact-loss events and fly-over segments are present. In such cases, finding the time instant within the periodic orbit, corresponding to the current surface of the workpiece at time t, can be achieved as

$$t_\tau = \min_m\{t - m\tau + lT \geq 0\},\ l = 0,1,2,\dots \tag{12}$$

where m is the lowest integer, when t_τ lands in a segment without fly-over. Consequently on the discrete mesh, the actual feed rate is

$$h(t_{j,i}) = m - {}^{1}u_{i,j} + {}^{1}u(t_{j,i,\tau}), \tag{13}$$

or 0 if $t_{j,i}$ is part of a segment in fly-over.

Generally $t_{j,i,\tau}$ will not land on an existing mesh point and ${}^{k}u(t_{j,i,\tau})$ has to be interpolated exploiting the same Chebyshev polynomials used for the spectral differentiation. Therefore,

$${}^{k}u(t_{j,i,\tau}) = \sum_{l=0}^{N-1} a_l \cos\left(l \arccos\left(2\frac{t_{j,i,\tau} - t_0}{\Delta t} - 1\right)\right), \tag{14}$$

where $t_0 = t_{m,1}$ and $\Delta t = t_{m,N} - t_{m,1}$ are the start point and length of the mth solution segment containing $t_{j,i,\tau}$. N is the degree of interpolation and the a_l coefficients are derived using discrete Chebyshev transform

$$a_l = \frac{1}{N-1}\left(\frac{1}{2}\left((-1)^l\,{}^{k}u_{m,1} + {}^{k}u_{m,N}\right) + \sum_{n=2}^{N-1} {}^{k}u_{m,n}\cos\left(l\pi\frac{n-1}{N-1}\right)\right). \tag{15}$$

In summary the formulated BVP consists of $n\times N\times m + n$ state variables ${}^{k}u_{j,i}$ and t_j (also ϕ if the excitation is harmonic), and the same amount of equality constraints, $n\times(N-1)\times m$ coming from (11), $n\times m$ from boundary conditions and n from event conditions shown in Table 1 (+1 phase condition).

3.3. Continuation algorithm

Due to the adaptive nature of the mesh and the complexity of calculating $h(t)$, for the solution of the previously formulated BVP, the *NLSolve.jl Julia* nonlinear solver package was employed [27]. For better convergence and numerical stability, an option to define extra segment boundaries one workpiece revolution after impact events (at $t_{\mathrm{imp}} + \tau$) was added. However, this option was seldom used, due to the increase of state dimension significantly slowing down the calculations.

Through the solution of the boundary value problem, single parameter continuation of hybrid periodic orbits became possible. By simple incremental modification of a system parameter, and repeated correction of the solution, branches of different families of periodic orbits could be followed. Since no saddle–node (fold) type bifurcations of periodic orbits are expected, only natural parameter continuation was implemented.

Unfortunately this continuation scheme has a few limitations. First, it requires rigorous initialization by defining the exact sequence of occurring events, which cannot change through the course of continuation, and second, the physical meaning of the orbits is not guaranteed by the equality constraints of the BVP alone. Consequently, additional inequality conditions must be defined and evaluated at every parameter step. The violation of these will indicate grazing bifurcations, where the continuation must be stopped and continued with a different sequence of events.

In the case of the impact event surface, two types of grazing bifurcation can happen. Either an already existing impact disappears, by the relative velocity reaching zero, or a new impact event appears, by the state reaching the event surface within the segments. These events can be detected by the violation of either

$$|{}^{4}u_{m,N} - {}^{3}u_{m,N}| > 0 \quad \text{or} \quad |{}^{2}u_{j,i} - {}^{1}u_{j,i}| < d, \tag{16}$$

where m marks all segments with impact boundaries at their end.

The situation is similar for the contact-loss event surface. An existing pair of contact-loss events and the enclosed fly-over segment might disappear, by the length of the segment becoming zero, or a new fly-over section might emerge from a breach of the event surface in an in-contact segment. These can be detected when

$$h(t_{m,i}) > 0 \quad \text{or} \quad |t_l - t_n| > 0, \tag{17}$$

is violated. Here m denotes all non-fly over segments, while l and n mark all possible combinations of contact loss event times. A similar condition to the second half of (17) was implemented between all segment boundaries to detect changes in the sequence of events.

Grazing events detected by all these inequality conditions can also be followed with the formulated continuation scheme. This is done in two parameters, by the introduction of an extra constraint and adding one of the system parameters to the state of the BVP. In case of turning with a constrained TMD, grazing bifurcations on the contact-loss event surface are the most important, as they indicate the margin of solutions with large amplitude vibrations and interrupted cutting, also known as chatter.

The extra condition was introduced on a new type of segment boundary, where to guarantee the grazing of the contact-loss event surface, apart from the $h(t) = 0$ condition, its derivative was also prescribed to be zero $\frac{\mathrm{d}}{\mathrm{d}t}h(t) = 0$. This assures a local extrema in feed rate and thus a grazing event. On discretized orbits, these conditions take the form shown in Table 1.

In some special cases an impact and a contact-loss grazing event were found to coincide, leading to a new segment boundary type, shown in Table 1 and Fig. 3 with colour blue. This event however, is only a by-product of the discretization scheme and the fixed order of non-smooth events. Nevertheless its two parameter continuation provided promising results, even though only two of its three existence conditions could be satisfied by the solution of the governing BVP.

4. Results

Working with piecewise-smooth systems is always a difficult and delicate task. To help speed up this process the numerical investigation of both models began with solving a large batch of initial value problems, to get a general sense of system dynamics. Based on the information gathered from these runs, searching for hybrid-periodic orbits became a lot easier.

Time domain simulations were also employed in the initialization phase of all continuation tasks, as the previously formulated BVP is highly sensitive of the initial state, especially when it comes to event times and event order. Consequently, the general order of investigation was to initialize an orbit by time domain simulation, correct and follow it to grazing events via continuation, then simulate new initial orbits and repeat the process until the target parameter domain is covered.

4.1. Quasi-frequency response function

First the simpler and easier to handle harmonically excited (4) case was examined. The most important and interesting characteristic of this model is its excitation frequency Ω dependence. In linear case, without constraints, this would be the frequency response function (FRF). Due to the nonlinearities arising from TMD collisions, this description is no longer valid, but the response amplitude's frequency dependence can still be investigated via hybrid periodic orbit continuation. Furthermore the phase and therefore the real and imaginary parts can also be approximated by applying the Hilbert transform on artificial time signals generated by the repetition of resulting periodic orbits.

Through continuation of different families of periodic orbits, quasi-frequency response functions (QFRFs) were formulated for the piecewise-linear vibro-impact oscillator, while varying system parameters between runs. The effect of dimensionless excitation

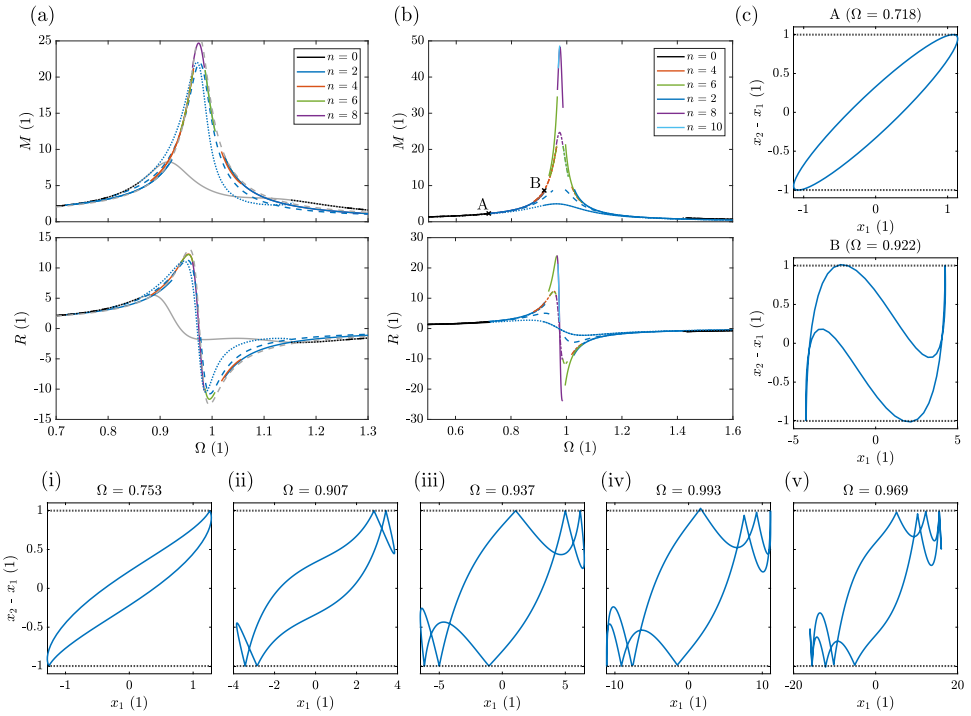

Fig. 4. Periodic orbit continuation results for the harmonically excited vibro-impact oscillator. Panel (a) presents the quasi-frequency response function (QFRF) on different excitation amplitudes (equivalent to modifying $\frac{1}{d}$), with $\mu = 0.05$, $\zeta = 0.02$, $r = 0.9$ and dotted: $f = 0.1$, dashed: $f = 0.2$, solid: $f = 0.5$. Here M is the absolute value and R is the real part of the dimensionless (quasi-)frequency response function ($\frac{1}{m_1\omega_1^2}QFRF$), Ω is the dimensionless excitation frequency and n is the number of impacts found in the followed orbits. The solid grey line shows the original, unconstrained linear FRF, while the dashed grey line denotes the effect of a Lanchester damper ($\chi \to \infty$). Panel (b) shows the same graph on different damping ratios, with $\mu = 0.05$, $f = 0.5$, $r = 0.9$ and dotted: $\zeta = 0.1$, dashed: $\zeta = 0.05$, dash–dot: $\zeta = 0.02$, solid: $\zeta = 0.1$. Panel (c) displays two critical, branch terminating, grazing orbits ($\mu = 0.05$, $\zeta = 0.02$, $f = 0.5$, $r = 0.9$), while panel (i–v) show periodic orbits with $n = 2$, 4, 6, 8, and 10 impacts. ($\mu = 0.05$, $\zeta = 0.01$, $f = 0.5$, $r = 0.9$). (For interpretation of the references to colour in this figure legend, the reader is referred to the web version of this article.)

amplitude f (which is inversely proportional to the TMD clearance d) and damping ratio ζ, is presented on Fig. 4(a) and (b). Concerning the rest of the parameters, μ and thus χ and φ were considered as given values, while r was found to have no noticeable effect on the shape of the function. Within orbits, the coefficient of restitution did not affect the vibration amplitude, only the number of impacts per period.

The original frequency response function is denoted by a grey line on Fig. 4(a). From the continuation results, it is clearly visible, that the system suffers a significant loss in damping performance if the displacement of the TMD is constrained. The negative peak of the real part cancelled out by Sims tuning [6] reappears. This will be shown to have severe consequences on the stability properties of the boring process.

The QFRFs take on a shape similar to the FRF of a slightly detuned 1 DoF system. This behaviour is similar to the one demonstrated in [28] for impact dampers, which states that on large vibration amplitudes the system behaves as if the moving mass was fixed directly to the vibration attenuated structure. Special dampers, where the stand alone damping ratio is regarded as infinite ($\chi \to \infty$), also known as Lanchester dampers, cause the two bodies to move in unison and produce a similar characteristics. This is demonstrated with a dashed grey line on Fig. 4(a).

For low f or high ζ values the QFRF can be constructed by following a single 2 impact, period 1 orbit. Changing these values leads to the quasi-frequency response function being segmented into multiple branches of different impact numbers by grazing bifurcations. For example a branch of 2 impact periodic orbits can terminate in the grazing events shown on Fig. 4(c).

There is a wide range of existing orbits, with a wide variety of impact numbers and orders. Due to the symmetricity of the system and the two impact surfaces, these are all either symmetric or come in mirrored pairs. The number of collisions increases with the vibration amplitude, theoretically up to infinity as Zeno behaviour and sliding solutions are reached [25]. The system can also exhibit more complicated behaviours, such as quasi-periodic solutions, but these were not investigated as the formulated numerical methods were unable to handle them.

Considering the intricacy and difficulty of uncovering all possible periodic orbits, the numerical investigation was restricted to symmetric orbits with even number of impacts, such as the ones presented on Fig. 4(i–v). Due to numerical limitations, initializing orbits becomes more and more difficult as the number of impacts increases. Consequently, only orbits with up to 10 collisions per period were considered. Nevertheless, despite all restrictions, following only these orbits was able to provide a reasonably full and accurate picture of system dynamics.

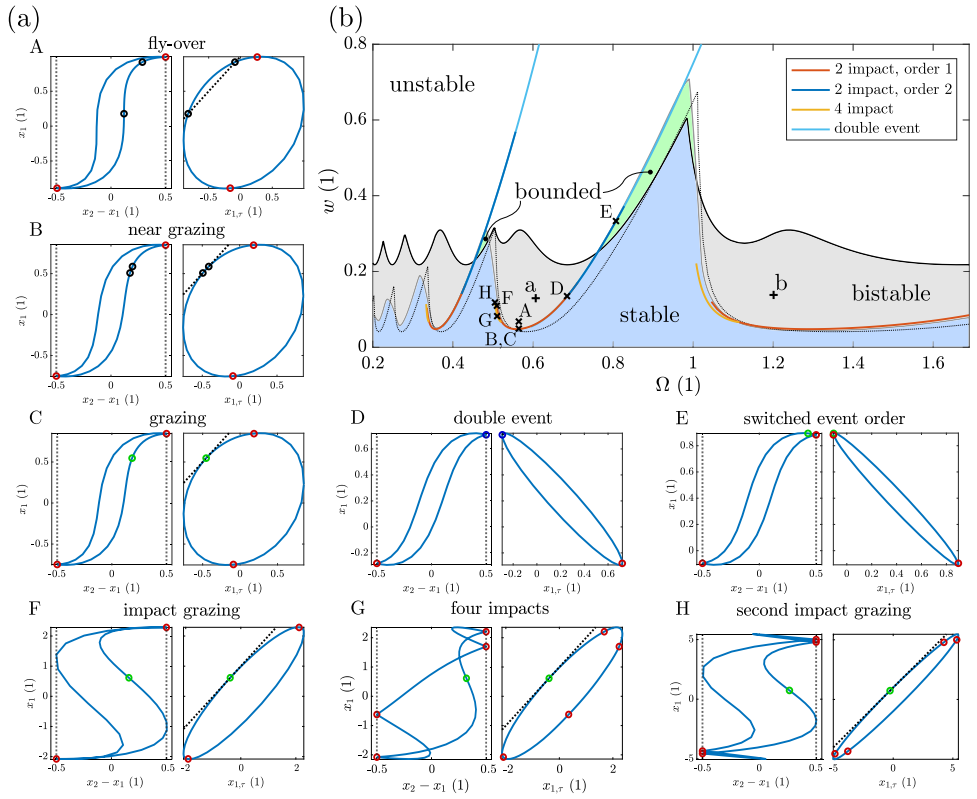

Fig. 5. Hybrid periodic orbit continuation results for turning with a constrained TMD (ζ = 0.02, μ = 0.05, r = 0.9, d = 0.5). Panel (a) shows the followed orbits. Starting with an initial 2 impact fly-over orbit, which is converted to a grazing orbit by single parameter continuation in w (A → B → C). Then it is followed in two parameters w, Ω, branching out to different more complicated orbits(→ D → E and → F → G → H). The colours black, red, green and blue denote the same events as in Table 1. Panel(b) shows the formulated "stability" map, where the blue and green areas have solutions without contact loss, the grey areas are bi-stable and the white area is unstable. Solid black line marks the linear stability map of 2 DoF turning, dotted black line the original 1 DoF turning, and grey line the contact loss limit derived by time domain simulations. (For interpretation of the references to colour in this figure legend, the reader is referred to the web version of this article.)

4.2. Stability map

If regenerative excitation (5) is present, uncovering all intricacies of system dynamics becomes even more complicated and time consuming. Consequently, the numerical investigation was focused only on determining parameter domains, which lead to machining operations with acceptable workpiece surface quality. In practice, this meant separating areas with solutions without contact-loss events and fly-over segments, from the rest of the parameter space.

This process was started by solving a large batch of initial value problems, within a binary search algorithm formulated for finding the minimal dimensionless depth of cut w necessary for cutting edge contact loss. A result of this search for a broad range of spindle speeds Ω is presented on Fig. 5(b) with a grey line.

Here the black line represents the linear stability map of turning with an unconstrained TMD. Parameter combinations below this line ensure the existence of a stable, constant steady state solution even for the constrained case. Nevertheless, it is found that given strict enough TMD displacement restrictions and large enough perturbations, even here (grey area), the system can exhibit steady state solutions with contact-loss events and fly-over. To ensure landing on such solutions large energy initial conditions were used for the aforementioned w limit search.

The other noteworthy result of the initial contact-loss limit search is the set of green areas of Fig. 5(b). Here despite the instability of the constant steady state solution, the TMD displacement constraints can limit the tool vibration amplitude to an acceptable level. Here the solutions take on a shape similar to the one shown for impact dampers in [11]. Segments with and without impacts follow one another in long periodic fashion, as the activation amplitude of impacting orbits is repeatedly reached then lost due the energy dissipated during collisions.

To validate the findings of the time domain simulation results, two parameter (w-Ω) continuation of contact-loss grazing orbits was implemented. This process followed the steps presented on Fig. 5(a). First the simplest possible type of orbit necessary for prolonged large amplitude vibrations was initialized through solving an initial value problem (A). Then this impacting, fly-over orbit was followed in w close to a contact-loss grazing bifurcation (B). Here the orbit was converted by replacing the two old

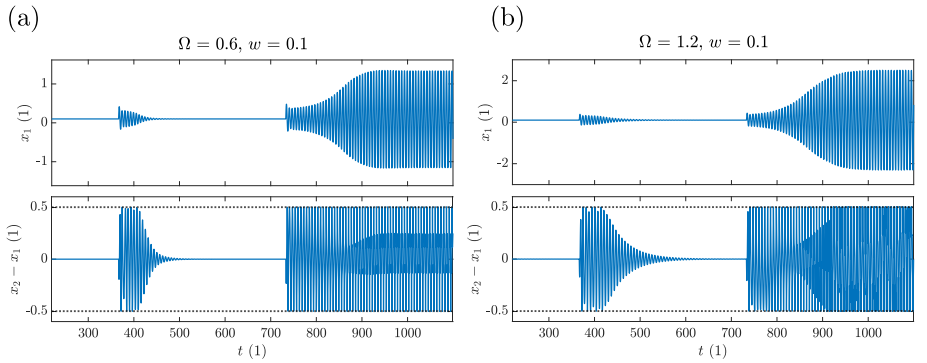

Fig. 6. Bi-stable behaviour of turning at point a and b of Fig. 5(b).

contact-loss events with a new grazing one (C). Then this orbit was followed in w-Ω, leading to an impact grazing event (F) and the overlap of two segment boundaries (D).

At the impact grazing event a new orbit was initialized through the same process as A → B → C, but now with 4 impacts (G). The continuation of this orbit lead to impact grazing events in both directions. The critical orbit (H) indicates that this process could be repeated for 6, 8 and so on impact orbits, making up the sections missing from the w limit on Fig. 5(b). Nevertheless, this was not performed considering the difficulty and tediousness of the task due to numeric limitations and parameter sensitivity.

At the other notable point (D) the continuation stops due to an inherent limitation of the algorithm, as events cannot change order or pass through one another. Here there are two possible ways to continue. Either a new double event is formulated (D), or the order of events is switched (E). Both solutions can be followed, however the latter will eventually lead to the former, as one of the impact events eventually converges to the contact loss grazing point as w is increased. Leading to the same issue as before with following C. The double event of D has 3 existence conditions, which cannot be satisfied simultaneously in two parameter continuation, however, the branch prescribing only the first two, coincides well with the time domain simulation results, thus validating them.

As seen on Fig. 5(b), the same continuation routine was repeated around $\Omega = 1.2$ and $\Omega = 0.335$ leading to similar results. Overall the time domain simulation and continuation results coincidence quite well.

4.3. Bi-stable behaviour of constrained TMDs

The bi-stable zones presented on Fig. 5(b) pose a significant danger, since here, even though linear stability analysis predicts safe operation, the system is prone to harmful chatter vibrations. Given large enough perturbations, the system no longer returns to its constant steady state solution, however, ends up on a stable impacting periodic solution with contact loss and fly-over effects.

Fig. 6 presents time domain simulation results, to illustrate this phenomenon. Two bi-stable w - Ω combinations were picked, point a and b from Fig. 5(b), with $\zeta = 0.02$, $\mu = 0.05$, $r = 0.9$, and $d = 0.5$. The system was perturbed by two impulses at $t = 366.52$ and $t = 733.04$, with the second one being slightly larger than the first. After the first disturbance, the system settles down to its constant steady state solution, however, the second one leads to exponentially growing vibrations which only become limited due to the onset of fly-over events and chatter.

Such impulsive perturbations are relatively common in manufacturing practice. Material impurities or geometric faults can often lead to sudden entry or separation of the cutting edge, producing impact like effects. Determining the systems explicit tolerance against these disturbances would go a long way towards optimal operation of boring bars with enclosed TMDs. Future work should be concentrated on this issue.

Modern machine tools contain a large number of moving parts, in the form of both passive and active elements, all subjected to some form of a motion limiting constraint. Such as finite strokes of e.g. inertial actuators, actuator or control saturations, end switches and geometric limits. Operating machines close to these boundaries can be unreliable and dangerous due to the arising non-smooth effects caused by reaching these rigid limits. Bi-stable behaviours similar to the one presented on Fig. 6 might arise leading to severe wear of moving parts and faulty machined workpieces.

The investigated displacement constrained passive tuned mass damper model provides an illustrative example on the dangers of non-smooth effects. The concept of avoiding collisions whenever possible can be generalized to all aforementioned devices, by staying clear of actuator and input saturations, actuator stroke limits, and geometric limits when operating industrial machine tools.

5. Conclusions

The effect of displacement limiting constrains is investigated on tuned mass dampers subjected to harmonic excitation and regenerative cutting force. Through time domain simulations and hybrid periodic orbit continuation, a quasi-frequency response function for a piecewise-linear vibro-impact oscillator, and a contact loss based stability map for boring with a constrained TMD is derived.

For this particular application, problem specific numerical schemes were constructed capable of handling both impact and contact-loss events, with special attention to Zeno behaviour and grazing bifurcations. Continuation of contact-loss grazing periodic orbits was found to be a reliable approach for determining stability boundaries in the non-smooth case of boring.

The arising collisions are shown to be inherently harmful for vibration attenuation. Despite the energy dissipated during impacts, the displacement constraints lead to a significant loss of attenuation performance. On the stability map of boring, major bi-stable zones appear, where large enough perturbations may lead to steady state solutions with contact loss, even though the constant steady state solution is stable.

Overall, tuned mass damper collisions are demonstrated to be a significant source of danger, which should be accounted for and avoided if possible when operating boring bars with enclosed TMDs.

CRediT authorship contribution statement

Zsolt Iklodi: Investigation, Software, Validation, Writing – original draft, Writing – review & editing, Visualization. **David A.W. Barton:** Methodology, Supervision. **Zoltan Dombovari:** Conceptualization, Supervision.

Declaration of competing interest

The authors declare that they have no known competing financial interests or personal relationships that could have appeared to influence the work reported in this paper.

Acknowledgments

This research was supported by the Hungarian Government in the framework of the NKFIH: 2019-2.1.2- NEMZ-2019-00005 and NKFIH FK 124361 research projects.

References

[1] A. Digernes, Damping Apparatus for the Damping of Vibrations, Google Patents, 2010, US Patent 7, 681, 869.
[2] D. Ostling, T. Jessen, Tool Body Including a Damping Apparatus and a Machining Tool Having Such a Tool Body, Google Patents, 2020, US Patent App. 16/652, 844.
[3] K. Sørby, Development and optimization of vibration-damped tool holders for high length-to-diameter boring operations, High Speed Mach. 2 (1) (2016).
[4] R. Rana, T. Soong, Parametric study and simplified design of tuned mass dampers, Eng. Struct. 20 (3) (1998) 193–204.
[5] J.P. Den Hartog, Mechanical Vibrations, Courier Corporation, 1985.
[6] N.D. Sims, Vibration absorbers for chatter suppression: A new analytical tuning methodology, J. Sound Vib. 301 (3–5) (2007) 592–607.
[7] H. Moradi, F. Bakhtiari-Nejad, M. Movahhedy, Tuneable vibration absorber design to suppress vibrations: an application in boring manufacturing process, J. Sound Vib. 318 (1–2) (2008) 93–108.
[8] M. Miguélez, L. Rubio, J. Loya, J. Fernández-Sáez, Improvement of chatter stability in boring operations with passive vibration absorbers, Int. J. Mech. Sci. 52 (10) (2010) 1376–1384.
[9] S. Ema, E. Marui, Suppression of chatter vibration of boring tools using impact dampers, Int. J. Mach. Tools Manuf. 40 (8) (2000) 1141–1156.
[10] R. Kasimani, T. Alwarsamy, S. Jayabal, Investigation of chatter stability in boring tool and tool wear prediction using neural network, Int. J. Mater. Prod. Technol. 46 (2013) 47–70, http://dx.doi.org/10.1504/IJMPT.2013.052789.
[11] E. Gourc, S. Seguy, G. Michon, A. Berlioz, B. Mann, Quenching chatter instability in turning process with a vibro-impact nonlinear energy sink, J. Sound Vib. 355 (2015) 392–406.
[12] S.W. Shaw, The dynamics of a harmonically excited system having rigid amplitude constraints, part 1: Subharmonic motions and local bifurcations, 1985.
[13] J. Shaw, S.W. Shaw, The onset of chaos in a two-degree-of-freedom impacting system, 1989.
[14] H. Tao, J. Gibert, Periodic orbits of a conservative 2-DOF vibro-impact system by piecewise continuation: bifurcations and fractals, Nonlinear Dynam. 95 (4) (2019) 2963–2993.
[15] D.J. Wagg, S. Bishop, Chatter, sticking and chaotic impacting motion in a two-degree of freedom impact oscillator, Int. J. Bifurcation Chaos 11 (01) (2001) 57–71.
[16] D. Wagg, Periodic sticking motion in a two-degree-of-freedom impact oscillator, Int. J. Non-Linear Mech. 40 (8) (2005) 1076–1087.
[17] P. Thota, H. Dankowicz, TC-HAT (TC): A novel toolbox for the continuation of periodic trajectories in hybrid dynamical systems, SIAM J. Appl. Dyn. Syst. 7 (4) (2008) 1283–1322.
[18] D.A. Barton, Stability calculations for piecewise-smooth delay equations, Int. J. Bifurcation Chaos 19 (02) (2009) 639–650.
[19] Z. Dombovari, D.A. Barton, R.E. Wilson, G. Stepan, On the global dynamics of chatter in the orthogonal cuttingmodel, Int. J. Non-Linear Mech. 46 (1) (2011) 330–338.
[20] R. Clewley, Hybrid models and biological model reduction with PyDSTool, PLoS Comput. Biol. 8 (8) (2012) e1002628.
[21] H. Dankowicz, F. Schilder, Recipes for Continuation, SIAM, 2013.
[22] L.N. Trefethen, Spectral Methods in MATLAB, Volume 10 of Software, Environments, and Tools, Vol. 24, Society for Industrial and Applied Mathematics (SIAM), Philadelphia, PA, 2000.
[23] J.P. Boyd, Chebyshev and Fourier Spectral Methods, Courier Corporation, 2001.
[24] C. Rackauckas, Q. Nie, Differentialequations.jl–a performant and feature-rich ecosystem for solving differential equations in julia, J. Open Res. Softw. 5 (1) (2017).
[25] A.B. Nordmark, P.T. Piiroinen, Simulation and stability analysis of impacting systems with complete chattering, Nonlinear Dynam. 58 (1) (2009) 85–106.
[26] K. Engelborghs, T. Luzyanina, K.I. Hout, D. Roose, Collocation methods for the computation of periodic solutions of delay differential equations, SIAM J. Sci. Comput. 22 (5) (2001) 1593–1609.
[27] P.K. Mogensen, K. Carlsson, S. Villemot, S. Lyon, M. Gomez, C. Rackauckas, T. Holy, D. Widmann, T. Kelman, D. Karrasch, et al., JuliaNLSolvers/NLsolve.jl: v4.5.1, Zenodo, 2020, http://dx.doi.org/10.5281/zenodo.4404703.
[28] M. Duncan, C. Wassgren, C. Krousgrill, The damping performance of a single particle impact damper, J. Sound Vib. 286 (1–2) (2005) 123–144.